

Angular directivity of diffracted wave in Bragg-mismatched readout of volume holographic gratings

A. Heifetz^{*}, J.T. Shen, S.C. Tseng, G.S. Pati, J.-K. Lee, M.S. Shahriar

Department of Electrical Engineering and Computer Science, Northwestern University, Evanston, IL 60208, United States

Received 3 March 2007; received in revised form 12 August 2007; accepted 15 August 2007

Abstract

We investigated theoretically and experimentally angular directivity of a diffracted beam in volume holographic gratings. We measured the angular direction of the diffracted beam as a function of Bragg-angle deviation of the read beam and showed that the experimental result agrees well with the Ewald sphere vector model (ESVM). We also showed that the Kogelnik's coupled-wave theory (CWT) is correct in predicting the diffraction efficiency, but is incomplete in its description of the direction of the diffracted wave. We show that the ESVM and the CWT theories taken together produce a self-consistent mathematical model of wave propagation inside the gratings that is confirmed with experimental results. The proper model for the direction of the output beam as presented here is important in developing theoretical models of image propagation through thick gratings for holographic imaging and correlation applications.

© 2007 Elsevier B.V. All rights reserved.

Holographic optical correlators offer potential advantages in speed for image processing applications, because of the inherent parallelism in optics [1,2]. An efficient implementation of a holographic correlator requires that the device performance be invariant to translations of the target in the field of view [3–5]. The underlying physics of shift-invariant correlation is Bragg-mismatched diffraction from holographic gratings. In designing shift-invariant holographic correlators, it is important to predict the exact angular direction of the diffracted beam in Bragg-mismatched readout of gratings. The direction of the diffracted beam is also important in developing the generic imaging properties of thick gratings [6,7].

In this paper, we derive the angular directivity using the Ewald sphere vector model (ESVM) [8–10] that matches with the experimental data very well. We also show that the angular direction of the diffracted wave in off-Bragg incidence is not predicted correctly within the framework of Kogelnik's coupled-wave theory (CWT) [11,12], because of the presence of phase factors that were not discussed in

the original derivation of the CWT. Nevertheless, the CWT is accurate in predicting the angular bandwidth of a volume holographic grating. We show that the ESVM and the CWT theories taken together produce a self-consistent mathematical model of wave propagation inside the gratings that is confirmed with experimental results.

Fig. 1 shows the model of a volume holographic grating which is used for our analysis. For simplicity, we restrict our attention to lossless transmission gratings; however the results presented here should also remain valid in the presence of loss. The z -axis is chosen in the direction of the wave propagation, the x -axis is in the plane of incidence and parallel to the medium boundaries, and the y -axis is perpendicular to the plane of incidence. In the general case the fringe planes are slanted with respect to the medium boundaries and the grating vector \mathbf{K} is oriented perpendicular to the fringe planes. The magnitude of the grating vector is $K = 2\pi/\Lambda$, where Λ is the period of the grating, and the angle of the grating vector is ϕ , measured with respect to the z -axis. The fringes of the grating are represented by a spatial modulation of the refractive index $n = n_0 + n_1 \cos(\mathbf{K} \cdot \mathbf{r})$, where n_1 is the amplitude of the spatial modulation, n_0 is the average refractive index, and \mathbf{r} is the position vector.

^{*} Corresponding author. Tel.: +1 847 467 0395.

E-mail address: a-heifetz@northwestern.edu (A. Heifetz).

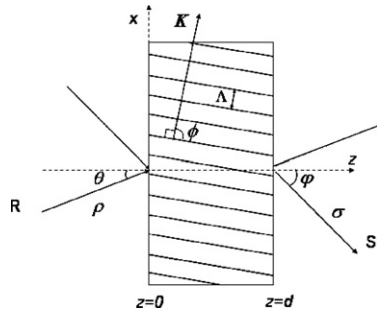


Fig. 1. Model of thick holographic gratings readout.

The read beam is denoted R and the diffracted signal beam S . The propagation vectors ρ and σ contain the information about the propagation constants and the directions of propagation of R and S , respectively. For Bragg-matched incidence, $|\rho| = |\sigma| = \beta$, where $\beta = 2\pi n_0/\lambda$ is the average propagation constant and λ is the wavelength in free space.

Vector diagrams illustrating Bragg diffraction are shown in Fig. 2 on the *Ewald* sphere, which is drawn on a plane as a circle of radius β . Bragg-matched readout is shown in Fig. 2 with dotted arrows. For Bragg-matched incidence, the propagation vector σ is related to ρ and the grating vector by

$$\sigma = \rho - K \tag{1}$$

corresponding to the most efficient phase-matching. For off-Bragg incidence, the vector relation takes the form

$$\sigma_E = \rho - K + \Delta\sigma \tag{2}$$

where $\Delta\sigma$ is a mismatch vector, which is introduced as a mathematical quantity in order to determine the direction of the diffracted beam.

In Bragg-mismatched readout, the diffracted beam is generated by the interaction of the electromagnetic field with the grating over an effectively semi-infinite volume. The uncertainty constraint for the diffracted beam can be written as $\Delta\sigma \cdot \Delta r \leq 2\pi$, where $\Delta\sigma$ represents the uncertainty in the diffracted beam wave vector σ_E and $\Delta r = \Delta x\hat{x} + \Delta y\hat{y} + \Delta z\hat{z}$ represents the dimensions of the region of interaction. The grating is assumed to be infinite in the x and y -directions, but has a finite thickness d in the z -direction. Furthermore, the spatial extent of the optical beam in the x and y -directions is assumed to be infinite under the plane-wave model. Even for the experimental situation, the extent of the beam in the x and y -direction is much larger than d . As such, we can assume that $\Delta x = \infty$, $\Delta y = \infty$, and $\Delta z = d$. Therefore, the bandwidth uncertainty product implies that $\Delta\sigma_x = 0$, $\Delta\sigma_y = 0$, and $\Delta\sigma_z d = O(\pi)$, so that $\Delta\sigma = |\Delta\sigma|\hat{z}$. The resulting vector diagram is shown in Fig. 2 with solid lines. That is, to obtain the direction of the diffracted wave in Bragg-mismatched readout, one should draw a vector in the z -direction from the tip of the $\rho + K$ vector to the surface of the *Ewald* sphere.

Next, we derive the angular direction of the diffracted beam wave vector for Bragg-mismatched readout using the mathematical formalism of the CWT. The reference and signal waves $R = R(z)\exp(-i\rho \cdot r)$ and $S = S(z)\exp(-i\sigma \cdot r)$ are described by complex amplitudes $R(z)$ and $S(z)$, which vary along the z -direction as a result of energy interchange. If the actual wave numbers differ from the assumed values, specified initially with ρ and σ , then mathematics will force these differences to appear in the phases of $R(z)$ and $S(z)$ in the final solution of the wave equation. The vector relation is shown in Fig. 3 on the *Ewald* sphere. CWT assumes that in case of Bragg-mismatched readout, the wave number is

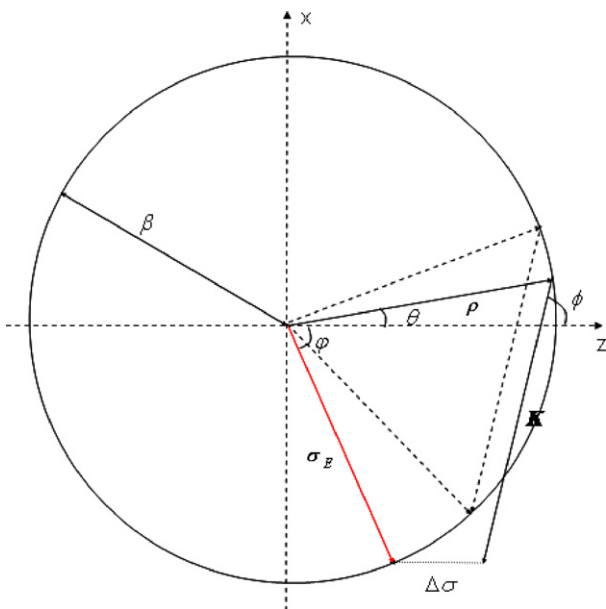


Fig. 2. Ewald sphere vector model diagram for Bragg-mismatched incidence.

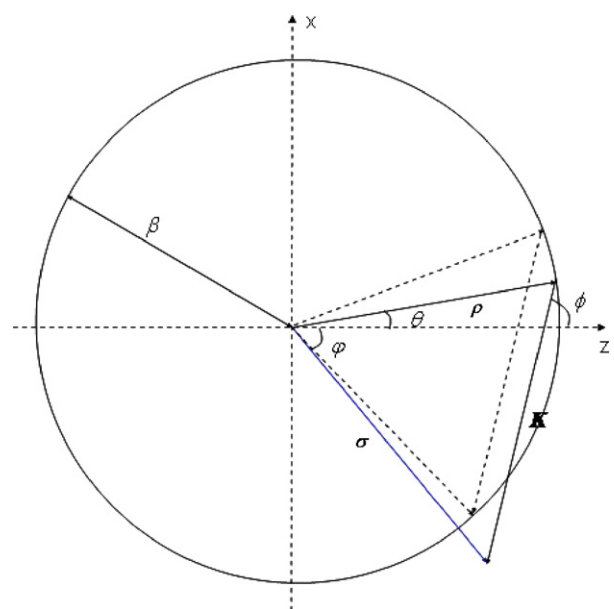


Fig. 3. Vector diagram illustrating the assumptions of the coupled-wave theory for Bragg-matched and Bragg-mismatched incidence.

$$S(z) = e^{i\frac{\Delta\sigma}{2}z} \left[-i\sqrt{\frac{c_R}{c_S}} \frac{v}{\sqrt{(\Delta\sigma/2)^2 + v^2}} \sin\left(\sqrt{(\Delta\sigma/2)^2 + v^2}z\right) \right] \quad (7a)$$

$$R(z) = e^{-i\frac{\Delta\sigma}{2}z} \left[i\frac{\Delta\sigma/2}{\sqrt{(\Delta\sigma/2)^2 + v^2}} \sin\left(\sqrt{(\Delta\sigma/2)^2 + v^2}z\right) + \cos\left(\sqrt{(\Delta\sigma/2)^2 + v^2}z\right) \right]. \quad (7b)$$

Note that the factor of $\Delta\sigma/2$ appears in Eq. (6) as a result of the exact solution of the coupled-wave equations, unrelated to the approximations preceding Eq. (6). Using the condition $\xi \approx \Delta\sigma/2$ from Eq. (6) leads to essentially the same expressions as in 3a and 3b

$$S(z) = -ie^{i\xi z} \sqrt{\frac{c_R}{c_S}} \frac{v}{\sqrt{\xi^2 + v^2}} \sin\left(\sqrt{\xi^2 + v^2}z\right) \quad (7c)$$

$$R(z) = e^{-i\xi z} \left[i\frac{\xi}{\sqrt{\xi^2 + v^2}} \sin\left(\sqrt{\xi^2 + v^2}z\right) + \cos\left(\sqrt{\xi^2 + v^2}z\right) \right] \quad (7d)$$

with the only difference that in Eq. (3) the phases of $R(z)$ and $S(z)$ are of the opposite sign. Just as in the discussion above, the phases of $S(z)$ and $R(z)$ introduce corrections to the initially defined wave-vectors. The corrected wave-vectors are

$$\begin{aligned} \sigma'_\xi &= \rho - \mathbf{K} + \Delta\sigma - \Delta\sigma/2 = \rho - \mathbf{K} + \Delta\sigma/2 \\ &\approx \rho - \mathbf{K} + \xi \end{aligned} \quad (8a)$$

$$\rho'_\xi = \rho + \Delta\sigma/2 \approx \rho + \xi, \quad (8b)$$

which are the same as the wave-vectors σ_ξ and ρ_ξ derived above.

Thus far we have presented three functional forms of the diffracted and transmitted beam wave-vectors in off-Bragg incidence. The first functional form is from the Kogelnik's CWT: $|\rho| = \beta$ and $\sigma = \rho - \mathbf{K}$ (Eq. (1)), which assumes efficient phase-matching but allows for $|\sigma| \neq \beta$. The second relation is our correction to the CWT: $\rho_\xi = \rho + \xi$ and $\sigma_\xi = \rho - \mathbf{K} + \xi$ (Eq. (5)) where $\xi = \hat{z}\Delta\sigma/2$. We have also shown that $|\sigma_\xi| \neq \beta$ and $|\rho_\xi| \neq \beta$. The third functional form derived from ESVM (and also used for alternative formulation of the CWT) is $|\rho| = \beta$ and $\sigma_E = \rho - \mathbf{K} + \Delta\sigma$ (Eq. (2)) where $\Delta\sigma = |\Delta\sigma|\hat{z}$. This relation does not assume efficient phase-matching a priori, but requires that $|\sigma_E| = \beta$. Note that regardless of the assumption on the initial value of the diffracted beam wave vector σ , the solution to the CWT forces the diffracted and transmitted beam wave vectors to become σ_ξ and ρ_ξ . This suggests that σ_ξ and ρ_ξ are the correct wave-vectors inside the gratings. In addition, we point out that the CWT solution to the diffraction efficiency, defined as $\eta = |c_S/c_R S|^2$, does not depend on the initial assumption of the value of σ . The diffraction efficiency obtained from either Eq. (3) or Eq. (7) is given by

$$\eta = \sin^2\left(\sqrt{v^2 + \xi^2}d\right) / (1 + \xi^2/v^2) \quad (9)$$

where $\xi = \Delta\sigma/2$ (as shown in Eq. (6)).

In order to see the implication of the foregoing analysis, it is instructive to consider explicitly the situation where the holographic grating with refractive index $n_0 + n_1\cos(\mathbf{K} \cdot \mathbf{r})$ is bounded by a uniform medium with a matched average refractive index n_0 on both the input and output sides, assumed in all of the foregoing analysis, and as shown in Fig. 5. According to the conventional interpretation of the Snell's law, which results from the requirement of continuity of the tangential components of the wave vectors at the boundary of two dielectric media, refraction is determined by the average refractive indices of the media. Since the average refractive index in the gratings is n_0 , Snell's law does not predict refraction of the beams at the matched index uniform slab/holographic grating boundary. However, we show that refraction does take place due to the spatial discontinuity of the index modulation term $n_1\cos(\mathbf{K} \cdot \mathbf{r})$. We refer to this process as the *holographic refraction*.

To understand this process, let us consider first the transmitted wave R . At the front end, the transmitted wave vector \mathbf{k}_R is in the direction of the unit vector $\hat{\rho}$, with an amplitude of β . According to the analyses presented above, \mathbf{k}_R inside the grating is in the direction of the unit vector $\hat{\rho}_\xi$ with an amplitude that differs from β . However, as this beam exits the back end, the amplitude of \mathbf{k}_R must again be equal to β . This fact, together with the boundary condition that the x and y components of \mathbf{k}_R remain unchanged throughout the whole process (see the discussion following Eq. (2)), implies that the transmitted wave will exit the back surface in a direction parallel to the incident \mathbf{k}_R vector, as shown by the dashed line in Fig. 5. Thus, the whole process

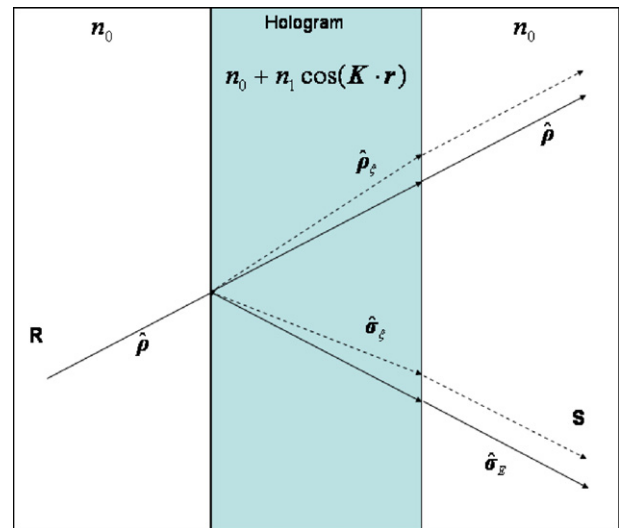


Fig. 5. Description of wave propagation inside the holographic gratings surrounded by a matching average refractive index medium. Solid lines inside the hologram show what the propagation of beams would be in a uniform glass slab. Dashed lines represent the actual directions of propagation of diffracted and transmitted beams inside the grating.

is equivalent to an effective refraction at both interfaces. The transverse shift of the outgoing beam expected from this model is too small to measure easily for the sample thickness of the order of 50 μm and a Gaussian beam with a waist size of about 1 mm. Note also that this model is consistent with the requirement that the direction of \mathbf{k}_R would follow the same path if incident from the right side, and exiting on the left side, due to the time-reversal symmetry of Maxwell's equations.

Consider next the diffracted wave S . Again, according to the analyses presented above, the diffracted wave vector \mathbf{k}_S is in the direction of the unit vector $\hat{\sigma}_\xi$, with an amplitude that differs from β . However, as this beam exits the back end, the amplitude of \mathbf{k}_S must be equal to β . This fact, together with the boundary condition that the x and y components of \mathbf{k}_S remain unchanged throughout this process, implies that \mathbf{k}_S vector will exit in the direction parallel to the unit vector $\hat{\sigma}_E$ (see Fig. 4), and shown by the dashed line in Fig. 5. As such, there is effectively a refraction of the diffracted beam as well at the exit surface. Of course, in our experiment, the medium outside the grating is air, with an index of ~ 1 . This leads to additional (conventional) refraction, which is taken into account in analyzing our experimental results.

Note that the model of the diffracted beam propagating in the gratings in the direction σ_ξ is consistent with the dependency of the diffraction efficiency η on $\xi = \Delta\sigma/2$. Since $\eta \propto |S|^2$, degradation in diffraction efficiency is the result of the diffracted wave vector dephasing inside the gratings. The diffracted wave vector σ_ξ is dephased by $\Delta\sigma/2\hat{z}$ from the efficient phase-matched wave vector σ (see Fig. 4). The wave-vectors ρ_ξ and σ_ξ cannot be measured inside the gratings, and outside the gratings the transmitted and diffracted wave-vectors change to ρ and σ_E . However, the diffraction efficiency is determined only by the diffraction inside the gratings.

One consequence of this model is that the wavelengths of the transmitted and diffracted beams inside the gratings are different, and neither is equal to $\lambda/n_0 = 2\pi/\beta$. For the particular case presented in Fig. 4, $\lambda_\rho > \lambda/n_0$ and $\lambda_\sigma < \lambda/n_0$. Note that the actual refractive index inside the hologram is $n = n_0 + n_1 \cos(\mathbf{K} \cdot \mathbf{r})$. Thus the transmitted wave “sees” an average refractive index smaller than n_0 , while the diffracted wave encounters an average refractive index larger than n_0 , due to a broken symmetry away from the Bragg-matched condition.

In order to test our theories, we performed an experiment designed to measure the angular deviation from the Bragg-angle of the diffracted beam $\Delta\varphi$ as a function of the angular deviation of the probe beam $\Delta\theta$. Our experiment was performed with a 50 μm thick Aprilis CROP photopolymer. We recorded the holographic gratings using an ND:YAG frequency doubled solid-state pumped Verdi laser operating at 532 nm. The writing beams R and S were incident on the hologram at 0° and 50° to normal in the air (see Fig. 1). We determined experimentally the angular bandwidth of the holographic medium to be equal to 2.5°

measured from null to null. To confirm that diffraction in our samples was in the Bragg regime, we calculated the values of $Q = 2\pi\lambda d/n_0\Lambda^2$ (Klein–Cook) and $\rho = \lambda^2/\Lambda^2 n_0 n_1$ (Raman–Nath) parameters [13,14]. Here $d = 50 \mu\text{m}$ is the sample thickness, $n_0 = 1.5$ is the average refractive index of the holographic medium, n_1 is the amplitude of the refractive index modulation, and Λ is the grating periodicity. We determined that $n_1 \approx 10^{-4}$ by measuring the diffraction efficiency at the Bragg-angle. We obtained $Q \approx 600$ and $\rho \approx 10^4$, which satisfy the conditions for the Bragg regime that both $Q \gg 1$ (thick grating) and $\rho \gg 1$ (weak modulation).

Fig. 5 shows the angular deviation from the Bragg-matched direction of 50° of the diffracted beam S for the read beam R scanning around Bragg-matched 0° incidence. The angles were corrected for the Fresnel refraction at the boundary of the holographic material in air. In the experiment, the reference beam R was fixed, and the grating was rotated so that the angle of incidence varied between $\pm 1.25^\circ$, and the angular deviation of the diffracted beam S was measured. For comparison, Fig. 5 displays the graphs obtained from the ESVM (Eq. (2)) (solid line), CWT (Eq. (1)) (dashed line), corrected CWT (Eq. (5)) (dotted line), and the experimental data (circles). The vector model graph matches the experimental data very closely, while the CWT and corrected CWT show a mismatch of up to 0.5 and 0.25° , respectively. To quantify data fitting, we calculated the slopes the (linear) theoretical plots, and of the linear fits to the experimental data obtained with coefficient of determination $R^2 = 1$, where R^2 is an indicator from 0 to 1 that reveals how closely the estimated linear trend corresponds to the actual data. The CWT, corrected CWT, ESVM, and the experimental data fits have slopes of $m = 1.11$, $m = 1.28$, $m = 1.45$, and $m = 1.41$, respectively, indicating that the ESVM curve provides the best fit to the experimental data. This is in agreement with our theoretical prediction. Note that measurement of the diffracted or transmitted beam directions inside the holographic gratings is potentially very difficult. Wave propagation inside the gratings is currently under investigation numerically with a finite-difference time-domain (FDTD) [15] method.

In addition, we investigated the accuracy of CWT in predicting holographic diffraction angular bandwidth. For lossless transmission gratings, the diffraction efficiency (Eq. (9)) depends on $\xi = \Delta\sigma/2$. However, the CWT would have predicted the correct direction of the diffracted beam only if $\xi = \Delta\sigma$, as can be seen by comparing Eqs. (2) and (5). To test this experimentally, we plotted normalized diffraction efficiency as a function of the incident beam angle in air for the theory curves (Eq. (9)) with $\xi = \Delta\sigma/2$ (solid line) and the experimental data (circles) in Fig. 6. For comparison, we also plotted normalized diffraction efficiency theory curve calculated with $\xi = \Delta\sigma$ (dashed line). The nulls of the diffraction efficiency of the CWT ($\xi = \Delta\sigma/2$) match very well with the experimental data, as expected. The angular bandwidth of the diffraction efficiency calculated under

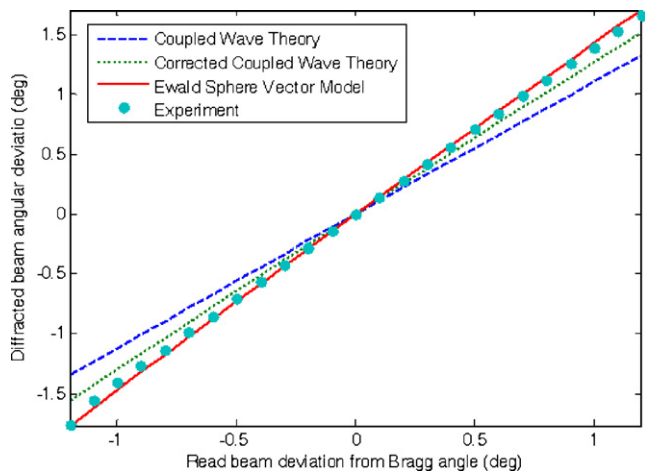


Fig. 6. Experimental and theoretical curves of diffracted beam angular deviation vs. read beam deviation from Bragg incidence for the read beam scanning around Bragg-matched angle of 0° . The curves are ESVM (Eq. (2)) (solid line), CWT (Eq. (1)) (dashed line), corrected CWT (Eq. (5)) (dotted line), and the experimental data (circles).

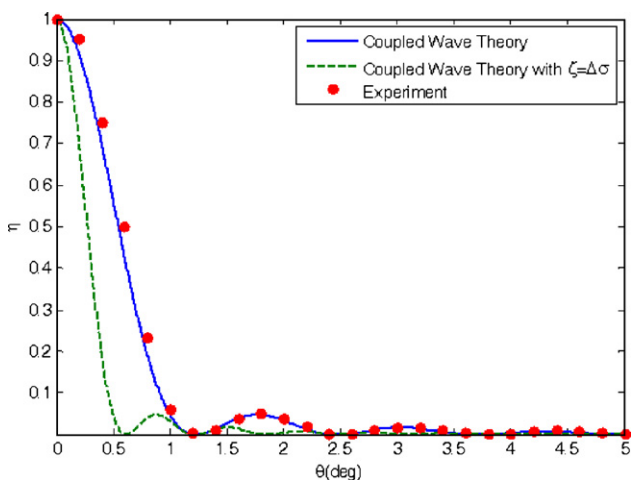


Fig. 7. Normalized diffraction efficiency as a function of the incident beam angle in air for the theory curves (Eq. (9)) with $\xi = \Delta\sigma/2$ (solid line) and $\xi = \Delta\sigma$ (dashed line), and the experimental data (circles).

the assumption that $\xi = \Delta\sigma$ is about one half of the experimentally observed angular bandwidth (see Fig. 7).

In summary, we investigated theoretically and experimentally the directionality of the wave vector of the

diffracted beam in off-Bragg readout of volume holographic gratings. We measured the angular deflection of the diffracted beam as a function of the deviation of the probe beam. We explained our experimental results on the basis of a *Ewald* sphere vector diagram. In addition, we obtained the theoretical expressions for the angular dependence of the diffracted beam wave vector and diffraction efficiency using the formalism of the coupled wave theory. We showed that the two theories taken together produce the correct description of the wave propagation inside the gratings. This analysis is important for construction of a working shift-invariant correlator, because one needs to be able to predict the direction of the correlation beam. Also, the results of this study are needed for developing a generic model for image transmission through a volume grating. This work was supported in part by AFOSR grant # FA49620-03-1-0408.

References

- [1] M.S. Shahriar, R. Tripathi, M. Kleinschmit, J. Donoghue, W. Weathers, M. Huq, J.T. Shen, *Opt. Lett.* 28 (2003) 525.
- [2] M.S. Shahriar, R. Tripathi, M. Huq, J.T. Shen, *Opt. Eng.* 43 (2004) 1856.
- [3] A. Heifetz, G.S. Pati, J.T. Shen, J.-K. Lee, M.S. Shahriar, C. Phan, M. Yamamoto, *Appl. Opt.* 45 (2006) 6148.
- [4] A. Heifetz, J.T. Shen, J.-K. Lee, R. Tripathi, M.S. Shahriar, *Opt. Eng.* 45 (2005) 025201.
- [5] J.W. Goodman, *Introduction to Fourier Optics*, third ed., Roberts and Company Publishers, 2004.
- [6] G. Barbastathis, D.J. Brady, *Proc. IEEE* 87 (1999) 2098.
- [7] Y. Takizawa, Y. Kitagawa, H. Ueda, O. Matoba, T. Yoshimura, *Jap. J. Appl. Phys.* 46 (2007) 605.
- [8] A. Adibi, J. Mumburu, K. Wagner, D. Psaltis, *Appl. Opt.* 38 (1999) 4291.
- [9] G. Barbastathis, D. Psaltis, *Volume holographic multiplexing methods*, in: H.J. Coufal, D. Psaltis, G.T. Sincerbox (Eds.), *Holographic Data Storage*, Springer, 2000.
- [10] B.Ya. Zel'dovich, A.V. Mamaev, V.V. Shkunov, *Speckle-wave Interactions in Application to Holography and Nonlinear Optics*, CRC Press, 1994.
- [11] H. Kogelnik, *Bell Syst. Tech. J.* 48 (9) (1969) 2909.
- [12] P. Yeh, *Introduction to Photorefractive Nonlinear Optics*, Wiley, 1993.
- [13] T.K. Gaylord, M.G. Moharam, *Appl. Opt.* 20 (19) (1981) 3271.
- [14] M.G. Moharam, L. Young, *Appl. Opt.* 17 (11) (1978) 1757.
- [15] A. Taflov, S. Hagness, *Computational Electrodynamics: The Finite Difference Time-domain Method*, third ed., Artech House, 2005.